IOPscience iopscience.iop.org

Home Search Collections Journals About Contact us My IOPscience

Experimental Raman scattering investigation of phonon anharmonicity effects in Li_2S

This article has been downloaded from IOPscience. Please scroll down to see the full text article.

1998 J. Phys.: Condens. Matter 10 2155

(http://iopscience.iop.org/0953-8984/10/9/018)

View the table of contents for this issue, or go to the journal homepage for more

Download details:
IP Address: 171.66.16.209
The article was downloaded on 14/05/2010 at 16:13

Please note that terms and conditions apply.

J. Phys.: Condens. Matter **10** (1998) 2155–2169. Printed in the UK PII: S0953-8984(98)88060-0

Experimental Raman scattering investigation of phonon anharmonicity effects in Li_2S

B Bertheville, H Bill and H Hagemann

Department of Physical Chemistry, Sciences II, University of Geneva, 30 Quai Ernest Ansermet, 1211 Genève 4, Switzerland

Received 1 October 1997, in final form 12 December 1997

Abstract. Experiments in which the Raman linewidth was measured as a function of temperature (7–1183 K) and pressure (0–400 bar) were performed on the (111) and (100) planes of single crystals of the cubic anti-fluorite Li_2S. The temperature dependence of the lattice constant was determined by x-ray diffraction (11–295 K). From these results and published Brillouin scattering data for this host, the volume thermal expansion coefficient as a function of temperature was obtained as well as the isothermal compressibility and the isothermal Raman mode Grüneisen parameter. Using the thermodynamic approach within the quasi-harmonic approximation, we show that below 400 K the volume effects describe well the temperature dependence of the Raman linewidth whereas above this temperature there are direct anharmonic effects appearing. Above approximately 850 K new Raman lines appear that are A_1 and E polarized.

1. Introduction

Ionic conduction in solids has aroused much interest in the last few decades because the underlying processes have widespread technical implications, such as in the construction of new and more efficient batteries and in the domain of solid-state chemical reactivity, especially at high temperatures. For these reasons an important research activity is going on in this field. Additionally, these investigations contribute to the theoretical and experimental understanding of the fundamental underlying mechanisms. Among the systems investigated, solid lithium-based ion conductors have excited much interest. Important issues from the applications side included high lithium-ion conduction in mixed glasses based on Li_2S, in binary sulphides (e.g. B_2S_3, GeS_2) and in other systems containing mixed Li_2S–lithium halides [1]. Comparatively very little work has been performed on the system Li_2S.

Lithium sulphide crystallizes in the face-centred cubic anti-fluorite structure with space group O_h^5 ($Fm3m$). The cations form a simple cubic Bravais lattice and the anions occupy the centre of one in every two cubes. This structure is antimorphous to the fluorite structure and therefore some similarity of the chemical and physical properties is expected. A most fascinating feature is the fact that both structures can undergo at high temperatures (but well below their melting point) a diffuse phase transition to a fast-ion-conduction region. This was first observed for the fluorite structure compounds CaF_2, SrF_2, BaF_2, PbF_2 and $SrCl_2$ [1–3]. Recent studies provided evidence that a similar transition does indeed occur also in anti-fluorite alkali sulphide compounds. Ionic conductivity experiments performed in our laboratory showed undoubtedly [4] the presence of this transition at around 1250 K in Na_2S ($T_m \simeq 1450$ K). Only recently, high-temperature experimental investigations and

0953-8984/98/092155+15$19.50 © 1998 IOP Publishing Ltd

theoretical studies were performed on the compound Li_2S. These include quasi-elastic neutron scattering work by Altorfer *et al* [5, 6] and Bührer *et al* [7], Brillouin scattering experiments by Mjwara *et al* [8], ionic conductivity experiments by Carron [9] and quantum mechanical Hartree–Fock studies by Lichanot *et al* [10]. These experimental and theoretical studies supply evidence for a substantial thermally induced disorder of the lithium sublattice near 850 K which could be accounted for by cation Frenkel defect generation. The work further furnishes precise data related to the thermal and elastic properties of Li_2S, which allowed us to analyse the anharmonic effects observed in our Raman scattering results. The cubic anti-fluorite structure involves, at the centre of the Brillouin zone, one allowed Raman line of T_{2g} symmetry. The cations vibrate in antiphase and the anions remain stationary. This line was studied as a function of temperature (7–1183 K) and of isotropic pressure (0–400 bar).

It is well known that a realistic crystal potential involves anharmonic contributions influencing importantly many thermodynamical properties of the crystal (see, e.g., [11, 12] and references therein). Usually these terms are treated as perturbations between the phonon modes (in [12, 13] and other references). Additionally, at higher temperatures thermally induced disorder effects perturb the phonon spectrum [13] and, in some cases, invalidate the phonon picture altogether. As the thermally induced disorder in the crystal destroys the adherence to the Raman selection rules of the perfect crystal and induces Raman scattering of other symmetries, we also performed high-temperature polarization experiments.

The isothermal Grüneisen parameter γ_j^T of the Raman phonon mode $j = T_{2g}$ obtained from the Raman pressure measurements together with the temperature dependence of the volume thermal expansion coefficient β determined with the aid of x-ray diffraction experiments and the volume compressibility κ extracted from published Brillouin diffusion experimental results allowed us to estimate the volume contribution (an implicit effect) to the T_{2g}-mode frequency shift ($\Delta\omega_j$) as a function of temperature within a Grüneisen–Mie approach. Furthermore, its comparison with the total frequency shift allowed us to gain insight into the anharmonic contribution (an explicit effect). Due to the proportionality to T^2 in the high-temperature limit, this latter effect gives measurable contributions to the temperature dependence of the observed Raman linewidth.

2. Experimental details

High-optical-quality single crystals of Li_2S were grown in our laboratory by the Bridgman technique. Details of the procedure have been given elsewhere [14]. High-quality single crystals of several cm^3 resulted. Samples with (111)-type faces were directly cleaved from the as-grown single crystals. Samples with (100)-type faces were obtained by cutting the Laue-oriented crystals. The surfaces were subsequently polished. Since Li_2S is a very hygroscopic compound, all of the operations were carried out under paraffin oil or in a glove box under an inert atmosphere. Typically, the sample length varied from about 3 to 5 mm.

The Raman set-up is laboratory constructed. It consists of a 5 W argon-ion laser, a 1403 SPEX double monochromator (maximum resolution 0.2 cm^{-1}) and a cooled 31034-A2 Burle low-level photomultiplier in conjunction with a Stanford Research dual-channel photon counter. Experiments were performed in the 180° scattering geometry and in general the argon-ion laser was operated at 488 nm, at a typical power of 0.04 W. This allowed us to minimize laser-heating effects. The Raman frequency shifts were accurately determined by measuring the Stokes and anti-Stokes components. The low-temperature Raman spectra

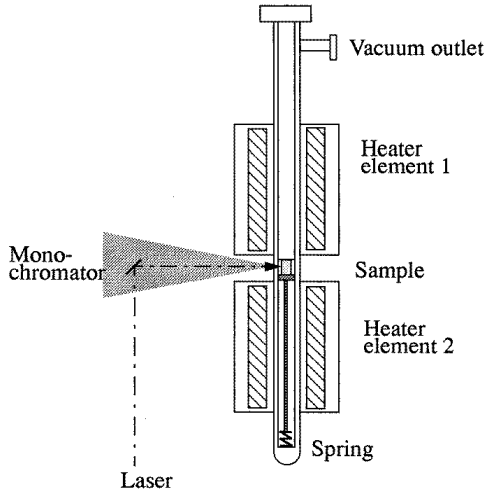

Figure 1. A schematic diagram of the Raman furnace and sample holder. The sample is squeezed between two platinum foils (not represented here) and measurements are carried out under a stabilized pressure of 0.2 bar of 5N argon.

were taken with the aid of an Oxford Instruments helium-flow cryostat in conjunction with a temperature controller. This controller measures and displays the temperature by means of an Au + 0.02% Fe, constantan thermocouple. Since the measured linewidths at low temperatures were very small, it was necessary to take into account the instrumental broadening. This was performed by recording spectra at different slit widths between 40 μm and 200 μm and by extrapolation to zero slit width. The high-temperature Raman measurements were realized with the aid of a home-built furnace (see figure 1). The design of the corresponding measurement cell containing the crystal was similar to the one previously reported [14] but was adapted to the new configuration of the furnace. At the highest temperatures ($T > 1100$ K), the large band thermal emission of the metallic sample holder prevented us from detecting the Raman signal efficiently. Furthermore, a slight deposition usually developed on the inner side of the quartz envelope and changes were noted on the crystal surface due to the reactivity of the sample. As a consequence the intensity of the Raman spectrum deteriorated over time. Several quartz tubes and single crystals were needed for fully investigating the temperature range.

The pressure mount consists of an EPR cavity used in the past for isotropic stress experiments. It is described in reference [15]. Pressures up to 400 bar were obtained by evaporating liquid argon into the closed system and were monitored by an analogue manometer (precision ± 5 bar). Several consecutive pressure measurement sequences were carried out to minimize the experimental errors. Since the Raman frequency shifts at those pressures are very small (maximum 1 cm^{-1}), the Raman spectra were recorded using a liquid-nitrogen-cooled CCD camera (ASTROLAB) at the exit of the SPEX 1403 monochromator. This arrangement allows one to eliminate the usual backlash problems encountered with a scanning monochromator. A density of 255 CCD pixels was available for the spectral range of 340–400 cm^{-1}. The entrance slit was set to 100 μm.

X-ray diffraction measurements were performed on Li_2S, as a function of temperature. An as-grown high-optical-quality single crystal was crushed into powder in our glove box (with a partial pressure of oxygen $\sim 10^{-2}$ Pa) and mixed with high-purity silicium. This

latter is used as an internal standard for the accurate determination of the cell parameter at very low temperatures. The experiments were performed with the aid of a HUBER G645 low-temperature powder diffractometer (Cu Kα_1 radiation) and the Rietveld method (program: FULLPROF [16]) was applied.

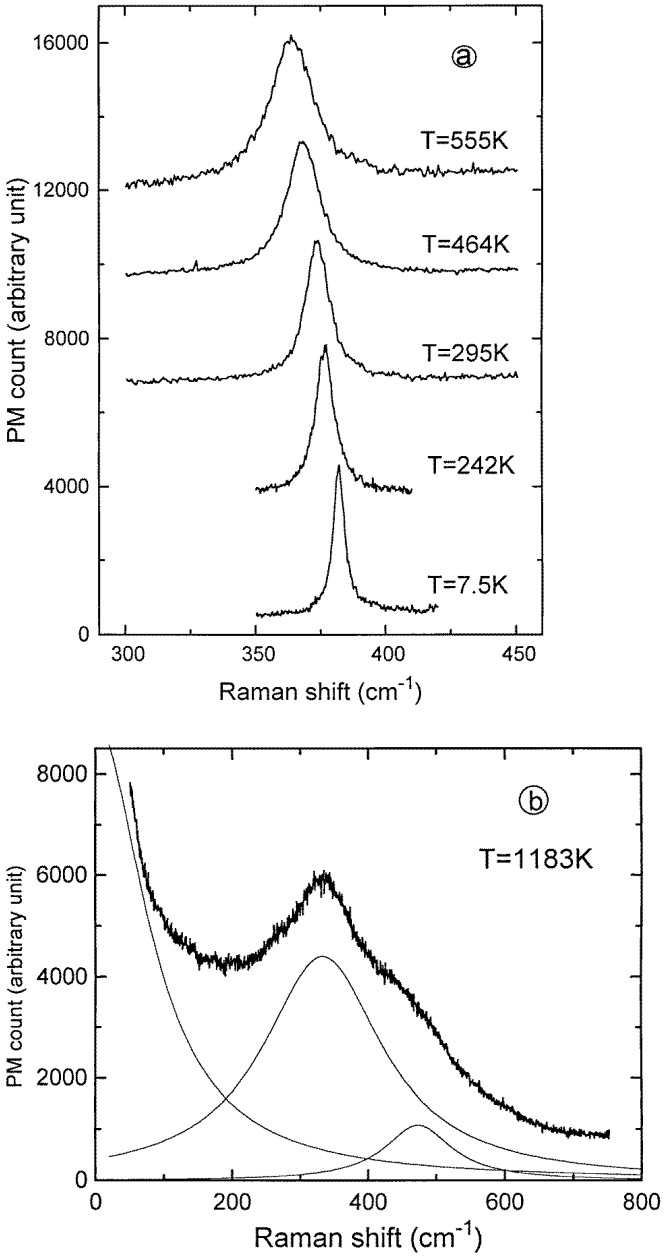

Figure 2. Unpolarized Raman spectra of the T_{2g} phonon mode in Li_2S single crystals at various temperatures: (a) below 850 K; (b) above this temperature.

Table 1. Structural, thermodynamical and spectroscopic parameters of several cubic anti-fluorite and fluorite compounds. All of the values refer to 300 K.

	Li_2S	Li_2O	CaF_2	SrF_2	BaF_2	PbF_2
a (Å)	**5.712**	4.619[h]	5.450[h]	5.782[h]	6.190[h]	5.935[h] (520 K)
β (10^{-5} K^{-1})	**5.564**	10.08[d]	5.70[a]	5.45[a]	5.60[a]	7.50[a]
κ (10^{-2} GPa^{-1})	**2.13**	1.225[e]	1.22[a]	1.43[a]	1.77[a]	1.65[a] 1.79[f]
$\omega_{T_{2g}}$ (cm^{-1})	**372.6**	523[d]	322[a]	286[a]	241[a]	256[b]
$(\partial\omega/\partial P)_T$ (cm^{-1} GPa^{-1})	**18.20**		7.30[c]	6.18[i] 7.00[c]	8.30[c]	
$\gamma_j^T = (1/\kappa\omega_j)(\partial\omega_j/\partial P)_T$	**2.30**	1.53[d]	1.88[a] 1.86[c]	1.51[i] 1.70[c]	2.00[a] 1.97[c]	
η	**1.92**	1.644[h]	1.436[g] 1.434[a]	1.440[g]	1.477[g]	1.778[g]

[a] Reference [26].
[b] Reference [29].
[c] Reference [30].
[d] Reference [31].
[e] Reference [32].
[f] Reference [33].
[g] Reference [34].
[h] Reference [35].
[i] Reference [25].

3. Results

3.1. Temperature and pressure dependence of the Raman signal

Figure 2(a) shows first-order backscattering Raman spectra of the allowed Raman T_{2g}-symmetry phonon line at different temperatures. They were obtained from (111)-cleaved single crystals of Li_2S. The positions and linewidths were determined by fitting the spectra with a Lorentzian function. The quality of the fit is better than ±3% up to 800 K. At 295 K, the frequency of the T_{2g} Raman mode was found to be 372.6 cm^{-1} with a full width at half-maximum (FWHM) of 10.8 cm^{-1}. The Raman signal shows at first the typical intensity decrease and line broadening with increasing temperature. However, above 850 K an asymmetric shape develops due to the fact that a second band appears on the high-frequency side. This latter band persisted up to the highest temperature investigated (1183 K). Figure 2(b) presents the spectrum observed at this temperature. Three main features of figure 2(b) should be emphasized: the very strong scattering intensity increase towards the elastic peak at the laser frequency, the remarkably large width of the T_{2g} line (200 cm^{-1}) and, finally, the presence of this high-frequency band. This situation in conjunction with the not especially good S/N ratio at high temperatures made a precise spectral decomposition difficult. It was therefore essential to perform polarized Raman experiments. They were carried out on (100)-polished single crystals with either an $x(yz)-x$ or an $x(zz)-x$ scattering geometry. Figure 3 shows results obtained at several temperatures. At temperatures above 850 K, the width of the T_{2g} Raman phonon line increases more rapidly than is predicted by the

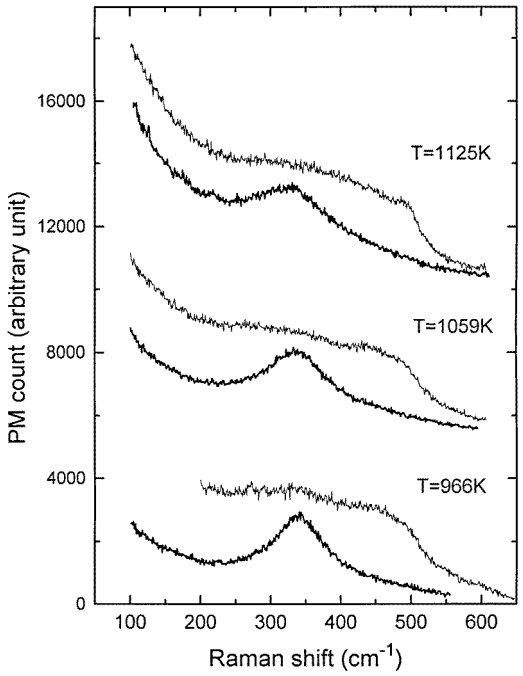

Figure 3. Polarized Raman spectra of Li_2S at different temperatures above 850 K. For each temperature, the upper curve corresponds to the A_1 and E contributions of the polarizability tensor and the lower curve to the T-symmetry contributions (the off-diagonal part of the polarizability tensor).

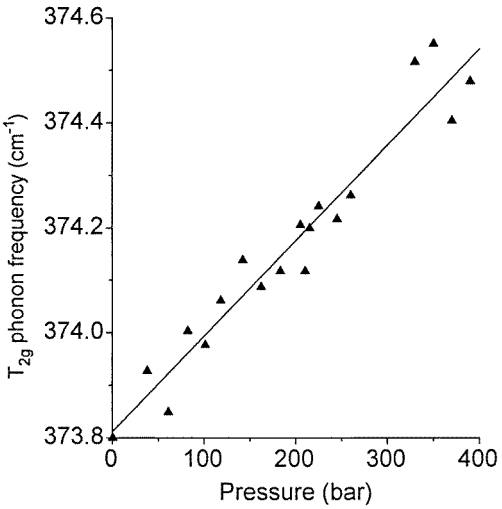

Figure 4. The pressure dependence of the T_{2g} phonon frequency of Li_2S at 300 K. The line represents the least-squares linear fit.

model discussed in this paper (see below). Simultaneously in this temperature range the supplementary high-energy band begins to appear in the Raman spectrum. The T_{2g} character

of the allowed (zone-centre) Raman line is well preserved above 850 K, whereas the new high-energy mode detected at 475 cm^{-1} is forbidden in the $x(yz)-x$ configuration. This agrees with the presence of $A_{1g} + E_g$ contributions to the scattering tensor of this latter band and of the broad feature. Note that the optical quality of these samples was less good than that of the freshly cleaved crystals. Still, the supplementary features are clearly identified above 850 K. The pressure dependence of the spectra was studied at 294 K. They were analysed by fitting a single Lorentzian through all of the data points between 340 and 400 cm^{-1}. Figure 4 gives the peak position as a function of pressure. The data are satisfactorily fitted by a linear relation (the continuous line in figure 5) with a slope $(\partial\omega/\partial P)_T$ of $+1.82$ (± 0.11) cm^{-1} $kbar^{-1}$. This value is more than twice that found for the fluorite compounds CaF_2, SrF_2, BaF_2 (see table 1). No measurable changes of the linewidth or of the Raman intensity were observed in the pressure range explored.

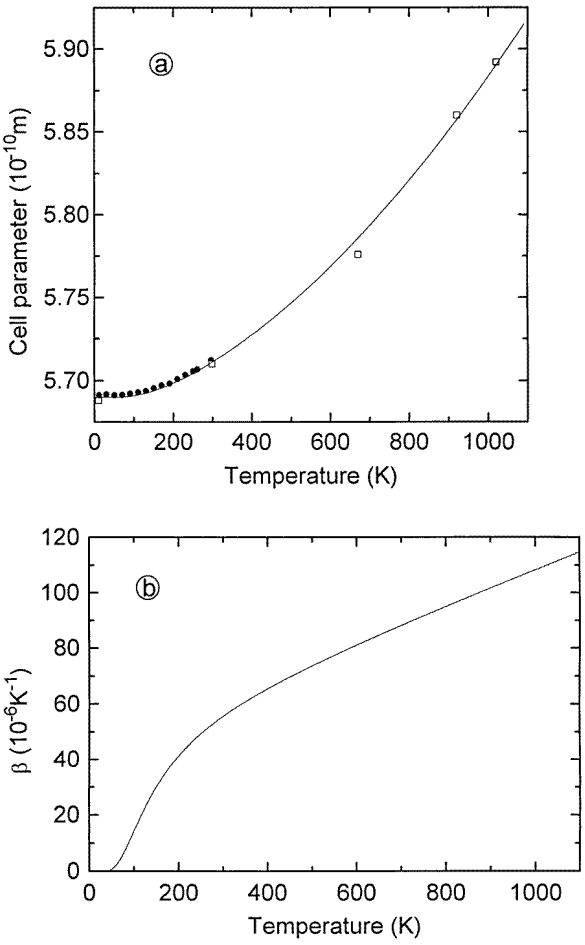

Figure 5. (a) The temperature dependence of the cell parameter of Li_2S between 0 and 1100 K. The open squares are experimental points from reference [7] . The solid line represents the best least-squares fit obtained by using equation (4). (b) The volume expansion coefficient β as a function of temperature obtained from equation (2).

Table 2. The lattice constant of Li_2S as a function of temperature determined by means of x-ray diffraction.

T (K)	a (Å)
11	5.6913(4)
30	5.6918(3)
50	5.6913(3)
70	5.6914(3)
90	5.6923(3)
110	5.6930(3)
130	5.6938(3)
150	5.6955(3)
170	5.6972(3)
190	5.6984(3)
210	5.7010(3)
230	5.7036(3)
250	5.7057(3)
260	5.7069(3)
295	5.7123(3)

3.2. Lattice parameters as functions of temperature

Within a thermodynamic model, the analysis of the phonon anharmonicity by Raman scattering requires knowledge of the temperature dependence of the volume thermal expansion coefficient β and of the bulk compressibility κ. The only relevant experimental data relating to the thermal expansion in Li_2S are those of Bührer *et al* [7], who determined with the aid of neutron diffraction experiments the dependence of the unit-cell parameter on temperature (15–1320 K). Since the number of experimental data points given there is small, in particular at low temperatures where the evolution of β clearly depends on temperature, we determined with our x-ray diffraction study the lattice parameter between 11 K and RT. Table 2 summarizes the results. The values found at 11 K and 295 K are in good agreement with those of reference [7].

4. Discussion

4.1. Determination of the thermal expansion coefficient, the bulk compressibility and the Raman mode Grüneisen parameter

On the basis of the temperature dependence of the lattice parameters, the linear thermal expansion coefficient α_L of Li_2S was then obtained as follows. We define [17]

$$\alpha_L = \frac{1}{a_0}\left(\frac{\partial a}{\partial T}\right)_p \tag{1}$$

where a_0 is the value of the cell parameter at zero temperature. Initially we tried to fit our data with a quadratic function of temperature. But the resulting linear variation $\alpha_L(T)$ at low temperatures was not satisfactory, since existing experimental data on the thermal expansion of fluorite showed a non-linear behaviour [18]. A much more satisfactory fit is obtained as follows. For a cubic crystal the linear thermal expansion coefficients along the three cubic axes are equivalent, and thus the volume thermal expansion coefficient (β) is given by $\beta = 3\alpha_L$. The experimental evolution of β between 0 K and 1100 K is described

by the following phenomenological analytical expression:

$$\beta(T) = \left[\frac{A}{T} + \frac{B}{T^2}\right] \sinh^{-2}\left(\frac{T_1}{T}\right). \tag{2}$$

This equation fulfils the basic requirement that $\beta \to 0$ as $T \to 0$. It is in part justified by arguments based on the lattice dynamics of anharmonic crystals [12, 19]. On the basis of the definition of α_L and the relation to β, the evolution of the cell parameter versus temperature can now be evaluated through

$$a(T) = \frac{a_0}{3} \int_0^T \beta(T)\ \mathrm{d}T + a_0. \tag{3}$$

The relation is readily integrated and one obtains

$$a(T) = \frac{a_0}{3}\left[\frac{AT_1(1 - \tanh^2(T_1/T)) + B\tanh(T_1/T)(1 - \tanh(T_1/T))}{T_1 \tanh^2(T_1/T)}\right] + a_0. \tag{4}$$

This result was fitted in a least-squares approach to the experimental temperature dependence of the lattice constant shown in figure 5(a). The following values of the constants were obtained: $A = 2.8 \times 10^{-3}$, $B = 2.026$ K, $T_1 = 209.5$ K and $a_0 = 5.69$ Å. The temperature dependence of β determined with the aid of equation (2) and by using these coefficients is shown in figure 5(b). As expected, β presents a physically meaningful asymptotic behaviour at low temperatures. Its value found at 300 K is 5.564×10^{-5} K^{-1} and this is quite similar to the one reported for the well-studied cubic alkaline-earth fluorides but is about half of the one found for Li_2O (see table 1).

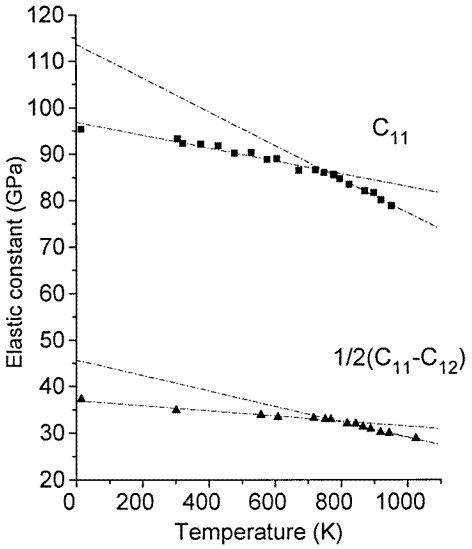

Figure 6. The temperature variation of the elastic constants C_{11} and C_{12} derived from the measured square of the Brillouin frequency shift, $(\Delta\omega_B)^2$, versus temperature, from reference [8].

For an isotropic cubic system, the bulk compressibility κ is related to the components of the elastic stiffness tensor C_{ij} (Voigt notation) by the relation

$$\kappa = \frac{3}{C_{11} + 2C_{12}}. \tag{5}$$

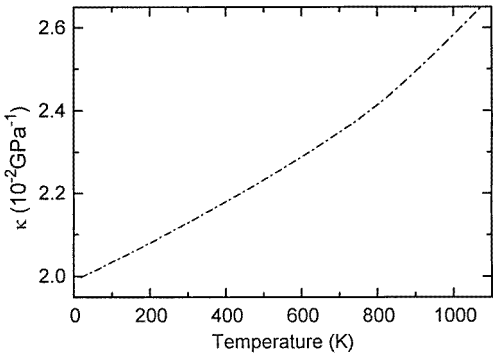

Figure 7. The bulk compressibility, κ, versus temperature. From equations (5) and (6).

The values at 15 K of the elastic constants C_{11} and C_{12} were determined from the initial slopes of the phonon dispersion curves measured at this temperature [7]. The results are 95.4 GPa for C_{11} and 20.9 GPa for C_{12}. Recent *ab initio* Hartree–Fock calculations [10] led to values of 94.1 GPa and 13.9 GPa. The agreement for C_{11} is very satisfactory (within 1%) whereas the off-diagonal C_{12} has very different values. As both the analysis of the experimental data and that of the numerical calculation involve simplifying assumptions, we use the average value of 17.4 GPa for C_{12} in the following. The temperature dependence of the C_{ij} was obtained by using the results of a recent experimental high-temperature Brillouin scattering study on Li_2S performed between 300 K and 1000 K [8]. The Brillouin frequency shift and the velocity of an acoustic mode propagating in a specific direction in a cubic crystal are related [20] by

$$\Delta\omega_B^2 = \frac{4\eta^2\omega_0^2 v^2}{c^2}\sin\left(\frac{\theta}{2}\right)^2 \tag{6}$$

where v is the velocity along the direction of propagation and ω_0 is the frequency of the exciting laser. The velocities necessary for the following discussion are given by $v_L = (C_{11}/\rho)^{1/2}$ (for [100]) and $v_T = [(C_{11} - C_{12})/2\rho]^{1/2}$ (for [110]). The experiments of reference [8] were performed with a scattering angle of 90° and at a wavelength of 488 nm of the incident light. In order to obtain precise values of C_{11} and C_{12}, it was necessary to know the refractive index η of crystalline Li_2S at ω_0. We treated η as an additional adjustable constant, independent of temperature. This is an approximation, in particular above 850 K. But it is justified by the absence of reliable published data for this temperature range. The quantity η was determined by fitting equation (6) to the experimental data of figure 6, giving η_{Li_2S} (488 nm) $= 1.92 \pm 0.02$. Subsequently, we found a theoretically obtained value of $\eta_{Li_2S} = 1.905$, in good agreement with our result. This number was derived with the aid of a lattice dynamics model including electrostatic and short-range effects [21]. The data presented in figure 6 show two reasonably linear regions with a discontinuity of the respective slopes in the vicinity of 850 K. In agreement with the quasi-harmonic theory [22], the results for C_{11} and $(C_{11} - C_{12})/2$ were parametrized using linear functions of T. The dotted lines shown in figure 6 represent the best fit obtained. Special care was taken to get a satisfactory fit also at low temperatures.

Next, these results were used for the determination of the temperature dependence of κ. The resulting curve is presented in figure 7. Comparison of the RT value of κ with the equivalent quantity for the fluorite hosts listed in table 1 shows that Li_2S has a remarkably high bulk compressibility. This is particularly evident when SrF_2 and Li_2S (with practically

the same lattice constants) are compared. This high value of κ is in agreement with the steep slope of the pressure dependence of the Raman line position (figure 4).

Table 3. The Raman mode frequency, compressibility and isothermal Grüneisen constant as functions of temperature.

T (K)	$\omega_{T_{2g}}$ (cm^{-1})	κ (10^{-2} GPa^{-1})	$\gamma_j^T = (1/\kappa\omega_j)(\partial\omega_j/\partial P)_T$
18	379.86	1.998	2.401
55	379.62	2.014	2.381
97	379.15	2.033	2.361
118.5	378.70	2.043	2.352
139.5	378.27	2.052	2.345
160	377.65	2.062	2.337
201	376.25	2.081	2.325
242	374.57	2.101	2.313
295	372.57	2.127	2.297
361	369.37	2.160	2.281
467	365.15	2.215	2.250
540	359.37	2.255	2.246
626	355.72	2.304	2.221
745	348.19	2.376	2.201
821	343.92	2.429	2.179
918	341.43	2.509	2.125
1002	338.05	2.584	2.083
1081	336.20	2.658	2.037

The isothermal Grüneisen parameter γ_j^T of the Raman phonon mode $j = T_{2g}$ is obtained from the slope of figure 4. In the quasi-harmonic approximation, ω_j is only a function of the volume of the crystal. Then γ_j^T is given by (Mitra [23])

$$\gamma_j^T = -\left(\frac{\partial \ln \omega_j}{\partial \ln V}\right)_T = \frac{1}{\kappa\omega_j}\left(\frac{\partial\omega_j}{\partial p}\right)_T. \tag{7}$$

By using the values of $\kappa(T)$ from equation (5) and the experimentally determined dependence $\omega_j(T)$, we calculated this mode Grüneisen parameter at different temperatures (see table 3). As there are no reliable data available on the temperature dependence of the slope of the Raman peak position versus pressure, it was assumed that this coefficient is independent of temperature ($(\partial\omega/\partial p)_T = (\partial\omega/\partial p)_{300\,K}$). The values of γ_j^T given in table 3 indicate a decrease of less than 10% between 200 K and 850 K.

4.2. Anharmonicity effects of the T_{2g} Raman line

The frequency, the intensity and the width of the T_{2g} Raman phonon line strongly depend on the crystal temperature as a consequence of the presence of anharmonic parts in the crystal potential energy. In a light scattering event, an incident photon $\hbar\omega_i$ is absorbed, leading to the creation of the Raman light quantum and an optical phonon $\hbar\omega_j$ which splits into several low-energy phonons because of anharmonic interactions. Different decay channels are opened by these contributions. The cubic anharmonic interaction allows for instance for the decay of one LO optical phonon into two LA acoustic phonons (a three-phonon interaction process), whereas the inclusion of the quartic anharmonic interaction may lead to the creation of three LA acoustic phonons (a four-phonon process). Several theoretical papers ([11–13] and references therein) showed that the principal effects arise from the

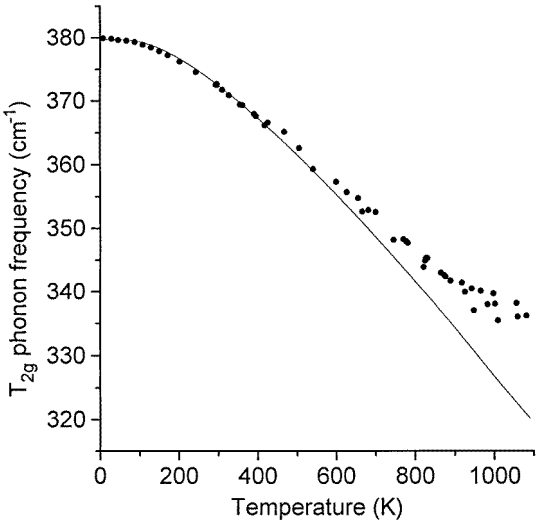

Figure 8. The temperature dependence of the T_{2g} phonon frequency. Full circles represent the experimental points and the solid line the volume contribution (implicit effect) due to thermal expansion of the crystal.

strains and the cubic and quartic contributions of the interaction potential. Within the quasi-harmonic approximation one determines a temperature-dependent set of crystal coupling parameters quadratic in the new displacement coordinates of the real strained crystal. To lowest order they are determined by the equilibrium of the strained crystal in conjunction with these effects of the third-order anharmonicity terms acting through the strains. The solutions of the associated equations of motion are modified phonons with frequencies depending on the volume (for cubic crystals). Then, by means of a perturbation calculation, one includes the direct coupling between these phonons via the dominant third-order and fourth-order anharmonic crystal potential parameters. When the lowest-order anharmonic interactions are taken into account in the radial interaction approximation, the temperature dependence of the Raman line position of an ionic crystal can be expressed as a sum of three contributions [24, 25]:

$$\omega_j(T) = \omega_j(0) + \Delta\omega_{j,vol}(T) + \Delta\omega_{j,anh}(T) \tag{8}$$

where $\omega_j(0)$ is the frequency at absolute zero of the jth vibrational mode of the real crystal, including the frequency of the ideal crystal in the harmonic approximation and a contribution due to disorder in the real crystal. The frequency shift $\Delta\omega_{j,vol}(T)$ is due to processes leading to thermal expansion of the crystal (a volume contribution or implicit effect), and $\Delta\omega_{j,anh}(T)$ is the frequency shift due to direct lattice anharmonicity contributions (an explicit effect). The shift $\Delta\omega_{j,vol}(T)$ can be estimated by using equations (7) and (2):

$$\Delta\omega_{j,vol}(T) = -\int_0^T \frac{\beta}{\kappa}\left(\frac{\partial\omega_j}{\partial P}\right)_T \mathrm{d}T. \tag{9}$$

We determined $\Delta\omega_{j,vol}(T)$ with the aid of the functions $\beta(T)$ and $\kappa(T)$ determined in this paper. The solid line in figure 8 represents the contribution of the sum $\omega_j(0) + \Delta\omega_{j,vol}(T)$ to the total shift of the phonon frequency, where $\omega_j(0) = 379.7$ cm^{-1}. The good correspondence between the curve and the experimental data below 400 K indicates that the frequency shift observed at these temperatures is indeed due to the volume effects. Above

this temperature it is necessary to include the anharmonic interaction, as its importance increases rapidly with temperature. Fourth-order anharmonicity causes a positive shift of the phonon frequency. This effect has already been reported for CaF_2, SrF_2 and BaF_2 [26].

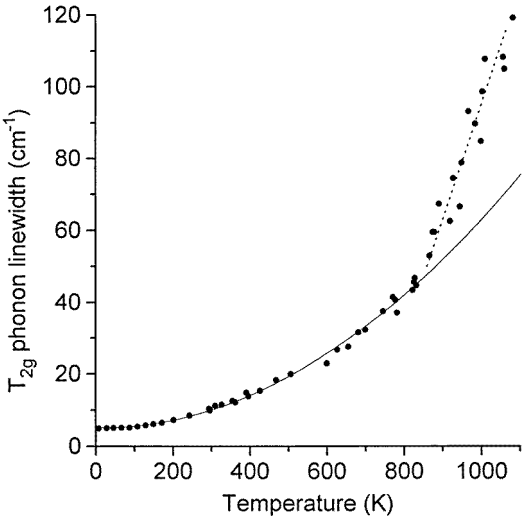

Figure 9. The Raman linewidth, Γ_j, of the T_{2g} lattice mode in Li_2S as a function of temperature. Full circles represent experimental data and the solid line is the best fit according to equation (10).

The temperature dependence of the linewidth obtained within this lattice dynamical perturbation approach indicates that, if only cubic anharmonic terms are considered, the linewidth increases linearly with increasing temperature, whereas if quartic anharmonic terms are included, a quadratic temperature dependence is predicted in the classical limit. An approximate analytical expression for the temperature dependence of Γ_j (the full width at half-maximum) was proposed [27, 28]. It is based on the assumption that only nearest-neighbour central forces are effective (see also the model proposed by Elliott *et al* [13]). This results in there being two coupling constants for a cubic crystal. A further assumption is that the frequencies ω_a and ω_b of the LA acoustic phonons produced by three- and four-phonon processes are $\omega_a = \omega_{LO}/2$ and $\omega_b = \omega_{LO}/3$. The linewidth is

$$\Gamma_j(T) = \Gamma_0 + a\left(n_a + \frac{1}{2}\right) + b\left[\left(n_b + \frac{1}{2}\right)^2 + \frac{1}{12}\right] \tag{10}$$

where Γ_0 is the residual broadening due to lattice imperfections (e.g. crystal defects), and $a/2$ (third order) and $b/3$ (fourth order) are the coupling constants producing the broadening of the phonon line at absolute zero due to the cubic and quartic anharmonicity, respectively. The phonon occupation numbers n_a and n_b are given by Bose–Einstein statistics. This approach contains additional approximations, such as the omission of other possible, more complex, decay channels and the assumption that all of the low-energy phonons have the same frequency. The solid line in figure 9 represents the best theoretical fit, obtained using (10). The values of the anharmonic constants a and b were found to be 0.572 cm^{-1} and 1.862 cm^{-1}, respectively, and the residual linewidth due to disorder in the crystal Γ_0 was found to be 4.21 cm^{-1}. Agreement between the theoretical and experimental values was obtained over the temperature range 0–850 K.

A similar behaviour of the T_{2g} phonon linewidth to that discussed above has already been reported by Elliott *et al* [13] for alkaline-earth fluorides. By including both anharmonicity and the effects due to defects (vacancies and interstitials) in a theoretical treatment of Raman scattering, they showed that a large concentration of defects could induce a breakdown of the selection rules and add a large broadening of the phonon linewidth.

Previous studies by Altorfer *et al* [5, 6] demonstrated that above 850 K the quasi-elastic neutron scattering observed from Li_2S was due to single-particle Li^+-ion motion. They further demonstrated, with the aid of diffraction data, that a large shift of the Li^+-ion position is observed along the $\langle 111 \rangle$ directions and that the octahedral interstitial sites are partially occupied. The question of whether the observed supplementary Raman bands are due to minute sulphur polymers deposited on the walls of the cell or whether they are genuinely due to the local trigonal clusters (C_{3v}) with the displaced Li ion and the vacancy located on the principal axis of the surrounding Li pseudocube remains to be resolved. The observed symmetry of the supplementary bands is not in contradiction with the hypothesis of such local clusters.

5. Conclusion

The temperature dependence of the one allowed T_{2g} Raman phonon mode in single crystals of Li_2S has been investigated in detail over the temperature range 7–1183 K. With the aid of x-ray diffraction experiments and Raman pressure measurements, the effects of the quasi-harmonic part associated with thermal expansion on the temperature dependence of the phonon frequency was studied. The results showed that these effects could not totally explain the experimental temperature dependence of the phonon frequency ω_j and linewidth Γ_j above 400 K. Fourth-order anharmonicity must be considered. Since a strong broadening of the T_{2g} line was pointed out above 850 K, as well as the appearance of a new high-frequency line, supplementary high-temperature polarized Raman experiments were performed. They demonstrated that supplementary scattering in normally forbidden symmetry is effective. The hypothesis of the onset of a possible diffuse phase transition in Li_2S remarkably far from its melting point ($T_m = 1645$ K) cannot be neglected.

Acknowledgments

This work was supported by the Swiss National Science Foundation (grant No 2-47163.96/1). The authors would like to express thanks to Dr W Bührer, Swiss Laboratory for Neutron Diffraction, PSI, Villingen, for a long-standing fruitful collaboration. They are also grateful to Dr R Cerny (Laboratoire de Cristallographie RX, Université de Genève) for performing the x-ray diffraction experiments. Mr F Rouge, Mr D Frauchiger and Mrs S Beuchat contributed at various stages of this study through crystal growth, mechanical and electronic construction work.

References

[1] Laskar A L and Chandra S 1989 *Superionic Solids and Solid Electrolytes* (New York: Academic)
[2] Lidiard A B 1974 *Crystals with the Fluorite Structure* ed W Hayes (Oxford: Clarendon)
[3] Hayes W and Hutchings M T 1989 *Ionic Solids at High Temperatures* ed A M Stoneham (Singapore: World Scientific)
[4] Bertheville B, Lovy D, Kubel F and Bill H 1997 *J. Phys. Chem. Solids* **58** 1569
[5] Altorfer F, Bührer W, Anderson I, Schärpf O, Bill H and Carron P L 1994 *J. Phys.: Condens. Matter* **6** 9937

[6] Altorfer F, Bührer W, Anderson I, Schärpf O, Bill H, Carron P L and Smith H G 1992 *Physica* B **180+181** 795
[7] Bührer W, Altorfer F, Mesot J, Bill H, Carron P and Smith H G 1991 *J. Phys.: Condens. Matter* **3** 1055
[8] Mjwara P M, Comins J D, Ngoepe P E, Bührer W and Bill H 1991 *J. Phys.: Condens. Matter* **3** 4289
[9] Carron P-L G 1990 *Thesis* University of Geneva
[10] Lichanot A, Aprà E and Dovesi R 1993 *Phys. Status Solidi* b **177** 157
[11] Maradudin A A and Fein A E 1962 *Phys. Rev.* **128** 2589
[12] Slaggie E L 1970 *Phys. Rev.* B **2** 2230
[13] Elliott R J, Hayes W, Kleppmann W G, Rushworth A J and Ryan J F 1978 *Proc. R. Soc.* A **360** 317
[14] Hagemann H, Clignez J-L, Rouge F and Bill H 1986 *J. Phys. E: Sci. Instrum.* **19** 199
[15] Moret J M and Bill H 1977 *Phys. Status Solidi* a **41** 163
[16] Rodriguez-Carvajal J 1990 *Satellite Meeting on Powder Diffraction, Congr. Int. Union of Crystallography (Toulouse, 1990)* abstracts, p 127
[17] Krishnan R S, Srinivasan R and Devanarayanan S 1979 *Thermal Expansion of Crystals* ed B R Pamplin (Oxford: Pergamon)
[18] Bailey A C and Yates B 1967 *Proc. Phys. Soc.* **91** 390
[19] Wallace D C 1972 *Thermodynamics of Crystals* (Chichester: Wiley)
[20] Comins J D, Ngoepe P E and Catlow C R A 1990 *J. Chem. Soc. Faraday Trans.* **86** 1183
[21] Pearson E W, Jackson M D and Gordon R G 1984 *J. Chem. Phys.* **88** 119
[22] Garber J A and Granato A V 1975 *Phys. Rev.* B **11** 3900
[23] Mitra S S 1965 *Phys. Status Solidi* **9** 519
[24] Liarokapis E, Anastassakis E and Kourouklis G A 1985 *Phys. Rev.* B **32** 8346
[25] Kourouklis G A and Anastassakis E 1986 *Phys. Rev.* B **34** 1233
[26] Samara G A 1976 *Phys. Rev.* B **13** 4529
[27] Vollis R F, Ipatova I P and Maradudin A A 1960 *Sov. Phys.–Solid State* **8** 850
[28] Sakurai T and Sato T 1971 *Phys. Rev.* B **4** 583
[29] Denham P, Field G R, Morse P L R and Wilkinson G R 1970 *Proc. R. Soc.* A **317** 55
[30] Mead D G and Wilkinson G R 1977 *J. Phys. C: Solid State Phys.* **10** 1063
[31] Ishii Y, Nagasaki T, Igawa N, Watanabe H and Ohno H 1991 *J. Am. Ceram. Soc.* **74** 2324
[32] Farley T W D, Hayes W, Hull S, Hutchings M T, Alba M and Vrtis M 1989 *Physica* B **157** 99
[33] Dickens M H, Hayes W, Hutchings M T and Kleppmann W G 1979 *J. Phys. C: Solid State Phys.* **12** 17
[34] Catlow C R A, Comins J D, Germano F A, Harley R T and Hayes W 1978 *J. Phys. C: Solid State Phys.* **11** 3197
[35] *CRC Handbook of Chemistry and Physics* 1993–1994 74th edn (Boca Raton, FL: Chemical Rubber Company Press)